Chapter 7

Spectroscopic Ellipsometry - Application on the Classification of Diamond-Like Carbon Films

XiaoLong Zhou and Hidetoshi Saitoh

Additional information is available at the end of the chapter

http://dx.doi.org/10.5772/intechopen.71727

Abstract

Diamond-like carbon (DLC) films have been spreading from their theoretical basis to worldwide industrial applications because of their unique properties. Since their properties depend strongly on the conditions of synthesis, the effective classification of DLC films becomes quite necessary. From the ternary phase diagram to the Japan New Diamond Forum standard, the classification attempts are also accompanied by the continuous development of their applications. Generally, the hydrogen content and $sp^3/(sp^2 + sp^3)$ ratio are the primary parameters for their classification. However, researchers are afraid that currently $sp^3/(sp^2 + sp^3)$ ratio estimated included not only network sp^3 but also sp^3 hybrid carbons in the hydrogen-terminated cluster. Simultaneously, the above classification methods need to use the large equipment, such as the synchronous radiation source. Therefore, to realize more straightforward to classify DLC films efficiently, the optical constants (refractive index (n) and extinction coefficient (k)) have been proposed in 2013 to be effective method to classify the DLC films, for which a lot of considerable discussion in the past ISO/TC-107 meetings has been made. The purpose of this chapter is to introduce the latest developments of optical constants on the classification of DLC films and explore their relationship with the current standard.

Keywords: spectroscopic ellipsometry, diamond-like carbon film, classification

1. Introduction

Diamond-like carbon (DLC) film is one of the attractive carbon materials due to its outstanding properties which have wide applications in mechanical, electrical, optical, and chemical fields [1]. In general, DLC films have complex structures composed of the "diamond-like" sp^3 hybrid carbons C(sp^3), sp^2 hybrid carbons C(sp^2), and hydrogen terminations [2, 3]. Many structural models have been proposed to describe the role of each component in DLC films.

One of the most famous models is the "two-phase structure model" which is proposed by Robertson [4]. This model considers that the DLC structure can be described as the C(sp^2) clusters embedded in the matrix of C(sp^3). The hydrogen terminations also play such an important role in all types of DLC films. Previous studies have emphasized that the bonding states of hydrogen atoms in the DLC films have been C(sp^3)-H in many cases [5]. When the hydrogen content exceeds a certain amount, the C(sp^3)-H bonds become close to the polyethylene (PE) structure where hydrogen atoms make the bonds with the sp^3 hybridized carbon atoms. Thus, the PE structure should also be taken into account as another phase of the DLC structural model. Then, a "three-phase model" might be appropriate to describe the DLC films which have certain hydrogen contents. With the continuous expansion of research, the effective classification of DLC films based on structural analysis becomes critical, because their properties depend strongly on the conditions and methods of synthesis [6]. In order to classify the DLC films systematically, various experimental methods have been used for structural analysis of DLC films. Raman spectroscopy, X-ray photoelectron spectroscopy, electron energy loss spectroscopy, near-edge X-ray absorption fine-structure (NEXAFS), solid-state nuclear magnetic resonance techniques, and Rutherford backscattering and elastic recoil detection analysis (RBS/ERDA) have been used to obtain the $sp^3/(sp^3 + sp^2)$ ratios or hydrogen contents of DLC films [3, 7, 8]. Based on these studies, the researchers in Germany and Japan have proposed a classification standard of DLC films in 2005 [9] and 2012 [10], successively. In this classification, DLC films are categorized into the four typical groups, so-called DLC films, type I : tetrahedral amorphous carbon (ta-C), type II: hydrogenated tetrahedral amorphous carbon (ta-C:H), type III: amorphous carbon (a-C), and type IV: hydrogenated amorphous carbon (a-C:H). And also other two special types, such as type V: graphite-like carbon (GLC) films and type VI: polymer-like carbon (PLC) films.

Nowadays, not only the structural analysis but also the physical, chemical, and mechanical properties have been used to distinguish the types of DLC films. Especially, the optical constants in terms of the refractive indices (n) and extinction coefficients (k) (at λ = 550 nm) measured by spectroscopic ellipsometry (SE) have been proved to be a simple and effective method to classify the DLC films. It was proposed in 2013 [11], for which a lot of considerable discussion in the past ISO/TC-107 meetings in 2016 (BSI, UK) and 2017 (Tokyo, Japan) has been made [12]. Since this method needs to use only an SE without the large-scale equipment (the hydrogen content was measured by the RBS/ERDA using an electrostatic accelerator [13], and the $sp^2/(sp^2 + sp^3)$ ratio was obtained by NEXAFS based on synchrotron radiation [2, 7, 14]), it is more conducive to simplify the classification of DLC films. However, it is necessary to discuss the consistency between the structural analyses made with SE and NEXAFS. In addition, Bruggeman effective medium approximation (BEMA) has been widely used to analyze the structure of DLC films [15, 16]. The BEMA theory is made up from the Lorentz-Lorenz equation based on a Lorentz local field theory and assumes the spherical dielectrics distributed in the mixed phases. In the BEMA equation, the dielectric function of DLC films (ε_a) can be approximated in terms of those of the selected specific standard materials. In the previous studies, graphite, highly oriented

http://dx.doi.org/10.5772/intechopen.71727

pyrolytic graphite (HOPG = PG in this chapter), glassy carbon (GC), diamond, PE, and void have been used as the standard materials. The ε_a can be obtained from the BEMA model simulations. Then, it is possible to analyze the structure of DLC films by fitting the spectrum measured by SE. However, the results of the previous analyses have been strongly dependent on the kind of the standard materials and their dielectric functions, and in addition, the types of DLC films have been limited to only a few species. Therefore, it is necessary to find the well-defined standard materials and the dielectric function of each standard material through the analysis of various types of DLC films.

In this chapter, we discuss the application of SE in the current classification of DLC films through two parts of experiments. In part one, DLC films were assumed to be represented by the superposition of the standard materials, for which the BEMA theory was applied to reproduce the experimental result of SE. From these analyses, the different types of DLC films can be represented by varying the superposition coefficients of the standard materials. We have selected five standard materials to build ten kinds of optical models after considering the feasibility of each model. In order to verify the reliability of the results, we used the X-ray reflectivity (XRR) method to measure the film densities as well as the NEXAFS method to evaluate the $sp^3/(sp^3 + sp^2)$ ratios and then compared the densities and ratios with that calculated from BEMA theory for individual films [14]. Finally, the discussion and comparison of the above methods are made on the structural analysis of various types of DLC films. In part two, we refurbished the classification of amorphous carbon films based on the optical constants (n and k). In the selected photon energy range, we defined the maximum of n ($E_{n\text{-max}}$) and k at a value more than 10^{-4} (E_k) to explore the relationship between the different classification schemes for amorphous carbon films deposited by different techniques [17].

2. Experimental details

In the part one experiment, 13 DLC films were prepared by different deposition methods which included samples provided by the other research groups upon the request by the authors. All the samples were deposited on a (100)-oriented p-type single silicon wafer substrate. Samples #01–03 were the provided samples which were deposited by a filtered cathodic vacuum arc (FCVA) method, and the detail conditions were unclear (to obtain ta-C films). Samples #04–06 were made by a FCVA method, where the graphite target (The Nilaco Co., Ltd., purity of 99.9%) was used as the carbon precursor at a negative bias voltage in the range of 1.0–2.0 kV, a deposition time of 10 min with a working pressure of 0.5 Pa, and an arc voltage of 800 V (to obtain a-C or ta-C:H films). Samples #07 and #08 were prepared by a radio-frequency (RF) magnetron sputtering method at a negative bias voltage of 0.3 kV, a deposition time of 5 and 3 min with a working pressure of 10 Pa, and a RF power of 150 W (to obtain ta-C:H or a-C:H films). Samples #09 and #10 were deposited by an electron-cyclotron-resonance chemical vapor deposition (ECRCVD) method at a negative bias voltage of 0.3 and 0.5 kV, a deposition time of 10 min with a working pressure of 0.5 Pa, and an RF power of

100 W (to obtain a-C:H or PLC films). Samples #11–13 were prepared by a plasma-enhanced (PE)-CVD method at the same 10-min deposition time and applied negative bias voltage in the range of 0.0–0.5 kV (to obtain a-C:H or PLC films). In the part two experiment, various types of DLC films were also deposited on a (100)-oriented p-type single silicon wafer substrate. Samples A–C were prepared by the FCVA deposition which is provided by the other research group upon the request of the authors. Samples D and E were deposited by RF magnetron sputtering at a negative bias voltage of 0.3 kV, a deposition time of 3 and 5 min with a working pressure of 20 Pa, and an RF power of 150 W. Samples F–K were synthesized by RF-PE-CVD methods at the same 10-min deposition time and applied negative bias voltage in the range of 0.0–0.5 kV.

All the DLC samples and the selected standard materials of PG and GC plates were measured with an ellipsometer (HORIBA, Jobin-Yvon, UVISEL NIR 23301010I). The incident angle of the source radiation was set to 70°; each measurement was carried out in the spectral range between 0.6 and 4.8 eV with a step of 0.05 eV at 293 K. The values of Tauc-band gap (E_g), n, and k are obtained from the fitting of the experimental data [18]. XRR was used to determine the true density and thickness of standard material GC and all the DLC films in the part one. In this approach, the X-ray was incident on the surface of the above materials at a small angle ($0.18° < 2\theta < 2.0°$), and the total reflection occurs at a critical angle. The XRR measurements (M03XHFMXP3, Mac Science) were taken by using a Cu $K\alpha$ source with the wavelength of 1.54 Å operated at an acceleration voltage of 40 kV and its currents of 15 mA under the condition of the scan range of 0.18–2.00° and the step size of 0.004°. The hydrogen content was evaluated by RBS/ERDA with 2.5 MeV He^+ irradiation using an electrostatic accelerator (Nisshin-High Voltage, NT-1700HS) located at the Extreme Energy Density Research Institute, Nagaoka University of Technology. The $sp^3/(sp^3 + sp^2)$ ratios of DLC films were obtained by NEXAFS method which was performed at the BL3.2Ub of the Synchrotron Light Research Institute (SLRI) (Public Organization), Nakhon Ratchasima, Thailand. The NEXAFS spectra were measured in the partial electron yield (PEY) mode, and the light polarization was parallel to the surface at any incident light angle. The total energy resolution was approximately 0.5 eV. The carbon K-edge NEXAFS spectra were measured in the energy range of 275–320 eV at an energy step of 0.1 eV. Absolute photon energy was obtained by adjusting the π^* (C = C) peak position of graphite. Uncertainty in the calibrated energy was estimated to be ±0.2 eV.

3. SE-BEMA analysis

3.1. Selection of standard materials

As described above, the main constituents in the structure of DLC films are C(sp^2), C(sp^3), and hydrogen terminations. Therefore, we selected the standard materials having these three basic structures individually as PG, GC, diamond, PE, and void. PG plate (NT-MDT, ZYA quality, GRAS/1.0) with the mosaic spread of 0.3–0.5° was used as the approximate crystalline

http://dx.doi.org/10.5772/intechopen.71727

C(sp^2) standard material. GC (Tokai Fine Carbon Co., Ltd., Grade GC-20SS) was used as the noncrystalline C(sp^2) standard material which was mirror-polished, and the surface roughness is 20 nm. We selected crystal diamond as the crystalline C(sp^3) standard material. Although several researchers [13, 14] used the sp^3-amorphous carbon to approximate the structure of C(sp^3), it was difficult to define the dielectric function and density of sp^3-amorphous carbon. Nonetheless, we used the dispersion equation of Sellmeier's formula (extinction coefficient, k = 0), [19]. For the structure of hydrogen terminations, previous studies pointed out that hydrogen atoms generally form –CH_n (n = 1, 2, and 3) groups with C(sp^3) which can be simulated by PE. We selected PE as the noncrystalline C(sp^3) standard material. The dispersion equation of classical oscillator model [20] used for the dielectric function of PE. In addition, the density and dielectric constant of DLC films were generally lower than those of crystalline diamond and graphite because of the amorphization and hydrogenation. This is due to the free volume formed during the film deposition process. For these reasons, we selected the void as one of the standard materials. The meaning of void has a wide variety, such as porosity and empty space. Guo et al. [21] have given the definition of the void as the existence of the free space resulting from incomplete interlocking of nuclei. There was no specific reference material so that we consider the permittivity of void approximately equal to the atmosphere as ε_r = 1.0 and ε_i = 0.

3.2. Optical model establishment

SE is an optical technique for investigating the dielectric properties of thin films, from which the film properties such as thickness, roughness, optical constants, electrical conductivity, compositions, and other material properties can be obtained. SE is an indirect method, that is, the measured amplitude component (Ψ) and phase difference (Δ) cannot, in general, be converted directly into the optical constants of a sample. Usually, a model analysis must be performed by using the models of Lorentz, Drude, classical dispersion, new amorphous, Tauc-Lorentz (TL) dispersion [18, 22], etc., which are used to fit and estimate the complex refractive index (dielectric function) of different materials. In these models, the Tauc-Lorentz dispersion formula has been the most commonly used to calculate the dielectric function of amorphous materials. The Levenberg–Marquardt algorithm has been used to check the fitting analysis of the (Ψ, Δ) spectra. The fitting error (χ^2) of each measurement was obtained from the difference between the experimental and simulated (Ψ, Δ) values [23]. The final result was obtained so as the χ^2 was considered to be the smallest in each fitting analysis. To determine the volume fraction and film thickness, the BEMA optical models were established to perform the simulation analyses based on the SE (Ψ, Δ) spectra. Considering that the model should be commonly applied to standard materials and all types of DLC films, we used the dispersion formula that combines Tauc-Lorentz (TL) and Drude models [23] (TL + Drude) to simulate the measured (Ψ, Δ) spectra. **Figure 1** shows all the optical models of standard material (**Figure 1(a)** for PG and (b) for GC) and DLC films (**Figure 1(c)–(l)**).

The simulation analyses of standard materials (PG and GC) were carried out before that of DLC films. For the PG, as shown in **Figure 1(a)**, the substrate was modeled by TL + Drude

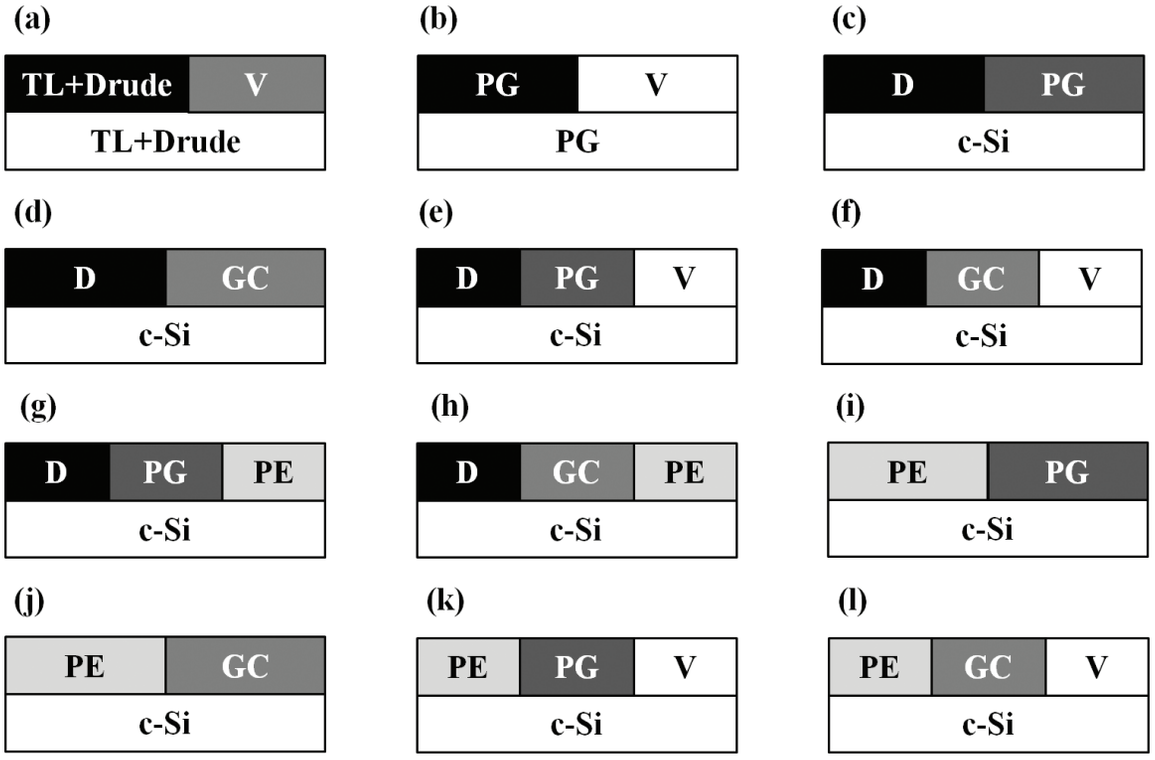

Figure 1. Optical models applied to BEMA equation (TL + Drude models, PG = HOPG, GC: glassy carbon, D: diamond, PE: polyethylene, and V: void). The models (a) and (b) are used for the simulation of PG and GC standard materials, the models (c)–(h) are used for the simulation of all types of DLC films, and the models (i)–(l) are used for the high hydrogen DLC films.

and the layer on the substrate was (TL + Drude) + void (50%). For the simulation of GC, which is considered to consist a certain amount of void and three-dimensional structural sp^2 hybrid carbon, the PG + void (50%) optical model with the BEMA screening factor $q = 0.333$ was used to fit the observed (Ψ, Δ) spectrum of the GC plate (roughness at 20 nm order). The dielectric function of PG and GC from these simulation analyses is shown in **Figure 2**. **Figure 2(a)** shows the Ψ and Δ spectra obtained for the measurement of PG plate and their simulated spectra by the dispersion equation of optical model (a). The observed spectra were fully reproduced by the simulated spectra, from which χ^2 of this simulation was 2.641, indicating that this optical model is appropriate to evaluate the dielectric function of PG. **Figure 2(b)** shows the comparison of the dielectric functions of PG obtained from the above analysis and Ref. [24]. As shown in **Figure 2(b)**, the present ε_r value shows any undulation at 0.9 eV which is observed in Ref. [24]. From the above results, we consider that the present dielectric function of PG can be used to build up the other optical models. **Figure 2(c)** shows the simulation of the GC based on the present dielectric function of PG. The χ^2 of the simulation was 4.845, which is larger than that of PG. Nonetheless, the observed and simulation data showed a good agreement. The comparison of the calculated dielectric functions and those of the GC reference [25] is shown in **Figure 2(d)**, from which it is indicated that the present dielectric functions of GC are closer to the reference functions than those of PG described above. The results suggest that our

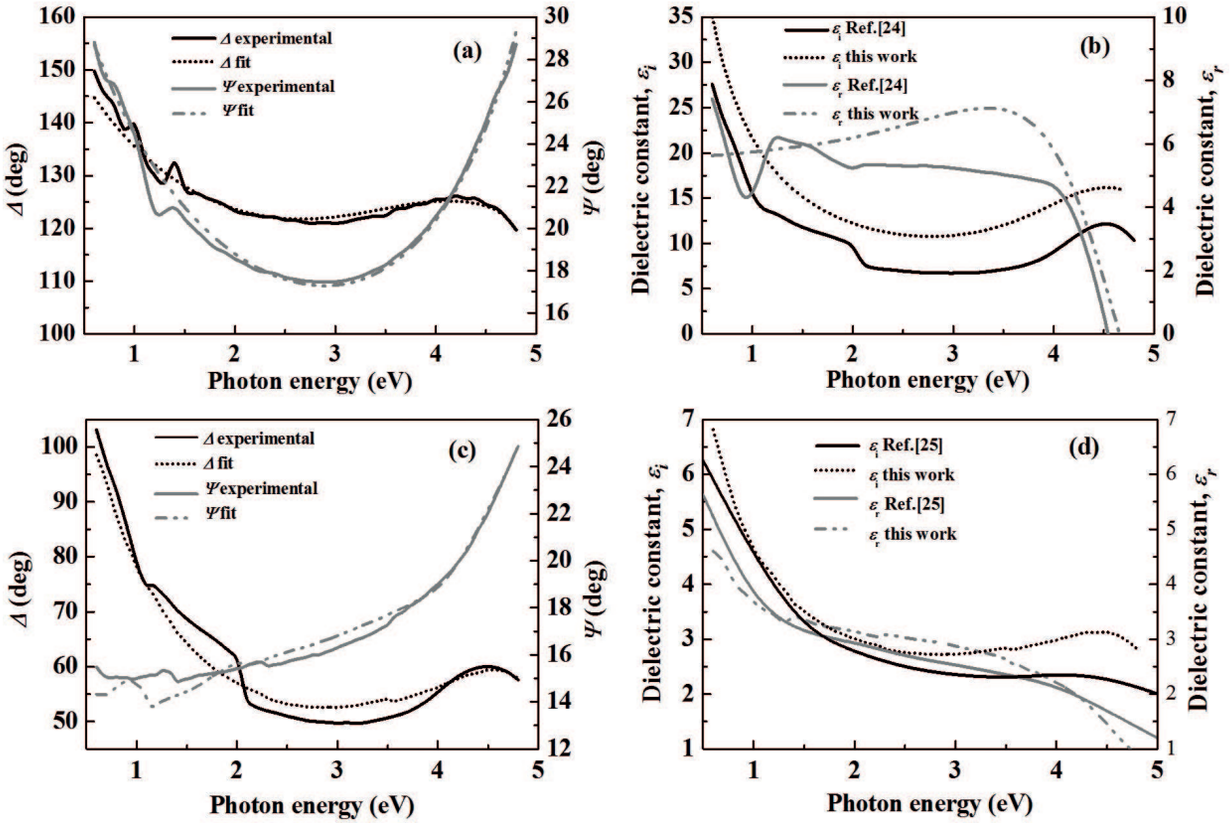

Figure 2. Simulation analysis of (Ψ, Δ) spectra and the resultant dielectric factions of PG and GC measured at the angle of incidence of 70. In (a) and (c), the solid line is the experimental Ψ and Δ spectra, and the dotted line is simulated Ψ and Δ spectra, respectively. In (b) and (d), the solid line is ε_r and ε_i functions, respectively, quoted from Ref. [24] for PG and Ref. [25] for GC, and the dotted line is those obtained from the present chapter.

analysis of SE using the BEMA theory and the selection of the standard materials of PG and GC are feasible in this chapter.

In the simulation of DLC films, we have assumed ten optical models as shown in **Figure 1(c)–(l)**. The crystalline silicon (c-Si) was used as the substrate in each optical model. The first layer of each optical model was assumed to consist of a mixed phase which was composed of several standard materials. The diamond or PE was assumed to be the standard materials of C(sp^3) component as well as PG or GC for the standard materials of the C(sp^2) component. For the free volume or hydrogenated termination, void or PE was assumed as standard materials in these optical models. Optical model (c)–(f) which have no PE phase contain with low hydrogen content should be suitable for types I, III, and V DLC films, especially, optical model (c) and (d) more suitable for ta-C or a-C films. Optical model (g)–(l) have the PE phase contain with hydrogen content in some degree should be suitable for types II, IV, and VI DLC films, especially optical models (k) and (l) more suitable for PLC films. In the first stage of these simulation analyses, all the DLC films were simulated by using the models of (c)–(h) where the diamond is one of the basic standard materials. However, the standard material of diamond cannot necessarily reflect the C(sp^3) structure for all kinds of the present DLC films, which can, instead, be represented well

Standard material	PG	GC	Diamond	PE	void
Density (g/cm^3)	2.26	1.69	3.52	0.95	0

Table 1. Densities of standard materials used for the analysis of the BEMA density.

by the PLC films when they are fabricated by PECVD or ECRCVD methods. In the second stage, therefore, the models (i)–(l) using PE as one of the basic standard materials are adapted to analyze the high-hydrogen content and low-density DLC films. In order to verify the correctness of the volume fractions of the individual components obtained by BEMA method and to validate the optical models used for the individual DLC samples, we calculated the BEMA density (ρ_{BEMA}) as:

$$\rho_{BEMA} = \sum_{i=1}^{3} \rho_i \times f_i. \quad (1)$$

In Eq. (1), ρ_i is the density of the standard material and f_i is the volume fraction. The ρ_i values are summarized in **Table 1**. Since the density of GC has been scarcely reported [26], we obtained the density of GC from the XRR measurement of a GC plate which will be described later. While the density of PE has a wide range of 0.91–0.96 g/cm^3 [27], the density of 0.95 g/cm^3 was used in this chapter which is closer to the high-density PE and DLC films.

4. Results and discussion

4.1. Results

In the part one experiment, the commercial software (Rigaku, GXRR) was used to simulate the logarithmic data of the reflection intensity, from which the density and thickness of GC and DLC films can be obtained. **Figure 3** shows the XRR profiles of the standard material of GC on a semilogarithmic scale. The solid curve represents the experimental profile, and the dotted curve the simulation analysis. In the high angle side (> 0.5°), there is a large discrepancy between the simulation and experimental curves. Nonetheless, the true density obtained from XRR method is generally determined by the critical angle, whose simulated value 0.358° is in good agreement with the experimental value 0.360°. The true density can be determined by the critical angle, and the thickness analyses by the fringe pattern which are obtained with GXRR software based on the Parrat's method [28]. Therefore, the discrepancy mentioned above in the large-angle region has no effect on the determination of the GC density. From the above measured critical angle of GC plate, the density is estimated to be 1.67 g/cm^3. Another measurement point yielded the density to be 1.71 g/cm^3. Then, the final density of standard GC was the arithmetic average of the two densities as 1.69 g/cm^3 in this chapter.

http://dx.doi.org/10.5772/intechopen.71727

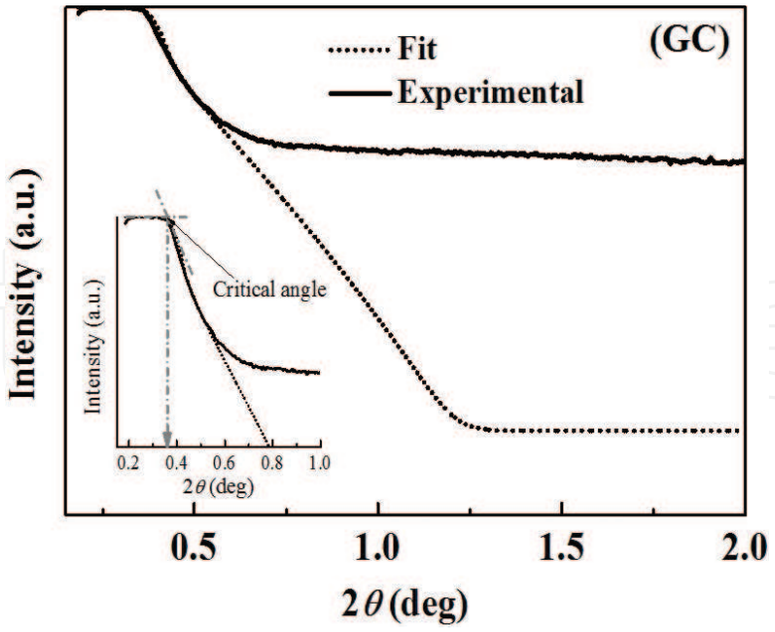

Figure 3. XRR profiles of GC (solid line: experimental profile, dotted line: fitted profile).

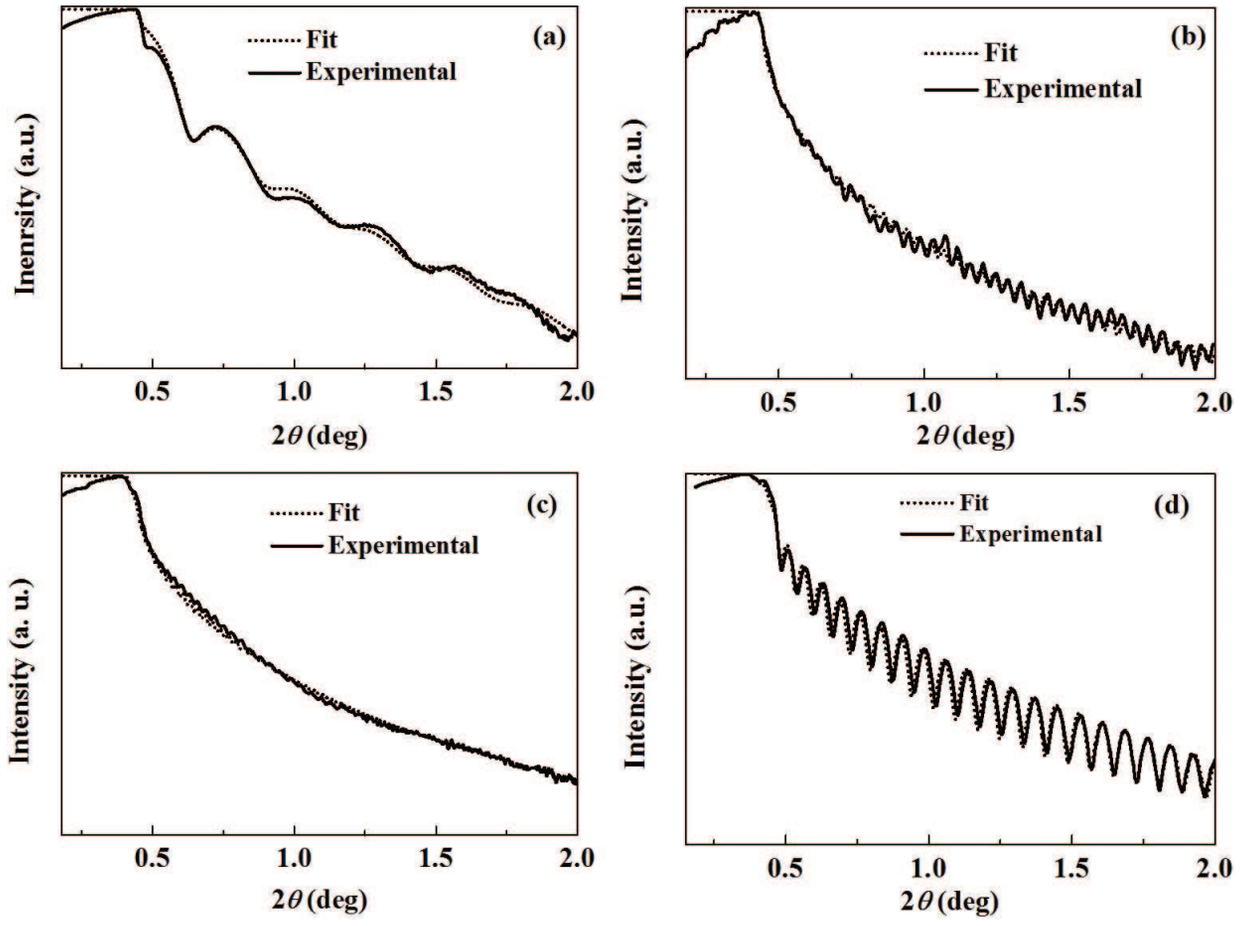

Figure 4. The XRR profiles of DLC films deposited from (a) FCVA #6, (b) sputtering #8, (c) ECRCVD #9, and (d) PECVD #12.

The examples of the XRR profiles and simulation results for the samples of #06, #08, #09, and #12 made by FCVA, sputtering, ECRCVD, and PECVD methods, respectively, are shown in **Figure 5**. The critical angles of these samples were 0.43, 0.40, 0.38, and 0.35°, from which the XRR densities (ρ_{XRR}) were 2.62, 2.21, 1.98, and 1.50 g/cm^3, respectively. Since the interferogram (the fringe in each XRR profile) appears periodically to change with the film thickness, the XRR thickness (d_{XRR}) of each film obtained from the fitting was 21.4, 188.8, 256.0, and 220.0 nm.

For all the other samples, ρ_{XRR} and d_{XRR} have also been obtained by the same way, and all the results are summarized in **Table 2**. Due to the variations of the deposition methods and the deposition time, d_{XRR} of deposited DLC films in this chapter is distributed between 21.4 and 312.0 nm. In addition, the film density was dependent on the film formation method. From these densities, the present DLC films can be classified as follows. The ϱXRR values of DLC films made by FCVA-I method are in the range of 3.02–3.25 g/cm^3, those of obtained from FCVA-II method are in the range of 2.01–2.62 g/cm^3, those of made by sputtering method are in the range of 2.17–2.21 g/cm^3, and those obtained from the ECRCVD and PECVD methods are in the range of 1.23–2.00 g/cm^3.

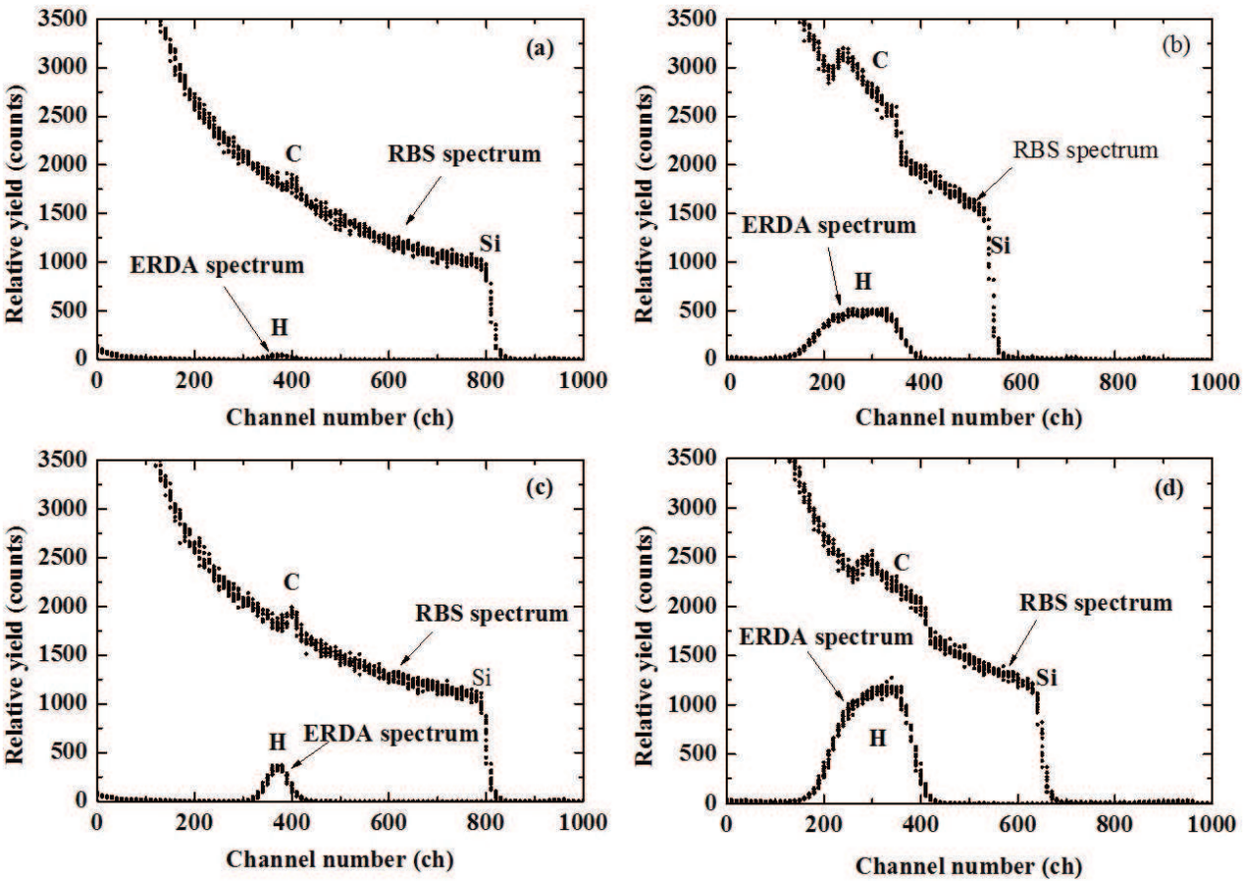

Figure 5. The RBS/ERDA spectra of DLC films deposited by (a) FCVA #6, (b) sputtering #8, (c) ECRCVD #9, and (d) PECVD #12.

http://dx.doi.org/10.5772/intechopen.71727

Sample	Method	d_{XRR} (nm)	ρ_{XRR} (g/cm^3)	ρ_{BEMA} (g/cm^3)	H content (at.%)
#01	FCVAI	181.0	3.10	3.23	0.3
#02	FCVAI	66.3	3.02	3.14	0.5
#03	FCVAI	210.8	3.25	3.17	1.0
#04	FCVAII	29.8	2.53	2.30	4.5
#05	FCVAII	26.9	2.01	2.01	4.5
#06	FCVAII	21.4	2.62	2.39	5.0
#07	Sputtering	312.0	2.17	2.15	19.0
#08	Sputtering	188.8	2.21	2.26	19.0
#09	ECRCVD	256.0	2.00	2.05	26.0
#10	ECRCVD	250.0	1.26	1.19	33.0
#11	PECVD	104.8	1.74	1.73	31.0
#12	PECVD	220.0	1.50	1.45	36.0
#13	PECVD	50.7	1.23	1.23	42.0

Table 2. Summary of d_{XRR}, ρ_{XRR}, ρ_{BEMA}, and hydrogen content of the DLC films.

Figure 5 shows the typical RBS and ERDA spectra of DLC films deposited by (a) FCVA #06, (b) sputtering #08, (c) ECRCVD #09, and (d) PECVD #12 methods. For the RBS spectra, the peaks that He^+ ions backscattered according to carbon atoms in DLC films are observed around 200–450 ch. For the ERDA spectra, the peaks of hydrogen atoms recoiled from the sample by the irradiation of He^+ ions emerged around 180–420 ch. The C and Si peaks on RBS spectra of the DLC films and the substrates are profiled using an RBS fitting calculation package. The H peaks on ERDA spectra of the DLC films are profiled using an ERDA fitting calculation package to compare the peak intensities of C and H. The estimating error of the present fitting process is around 5%. The hydrogen contents of DLC films of #06, #08, #09, and #12 were 5.0, 19.0, 26.0, and 36.0 at.%, respectively. **Table 2** lists the other results obtained from the above peak fittings. The hydrogen content of DLC film of type made by FCVA method was in the range of 0.3–1.0 at.% and that of type in the range of 4.5–5.0 at.%. The hydrogen content of DLC films obtained from sputtering method was 19.0 at.%. The hydrogen contents obtained from the ECRCVD and PECVD methods were in the range of 26.0–42.0 at.%.

Figure 6 shows the examples of the carbon *K*-edge NEXAFS spectra of DLC films synthesized by (a) FCVA #06, (b) sputtering #08, (c) ECRCVD #09, and (d) PECVD #12 methods. These spectra are decomposed into the two-edge structures. A pre-edge resonance near 285 eV is assigned to the transition from the C 1 *s* orbital to the unoccupied π^* orbitals principally originating from sp^2 or *sp.* sites if present. The other broadband between energy edges from 288 to 320 eV is related to the C 1 $s \rightarrow \sigma^*$ transitions at the *sp.*, sp^2, and sp^3 sites

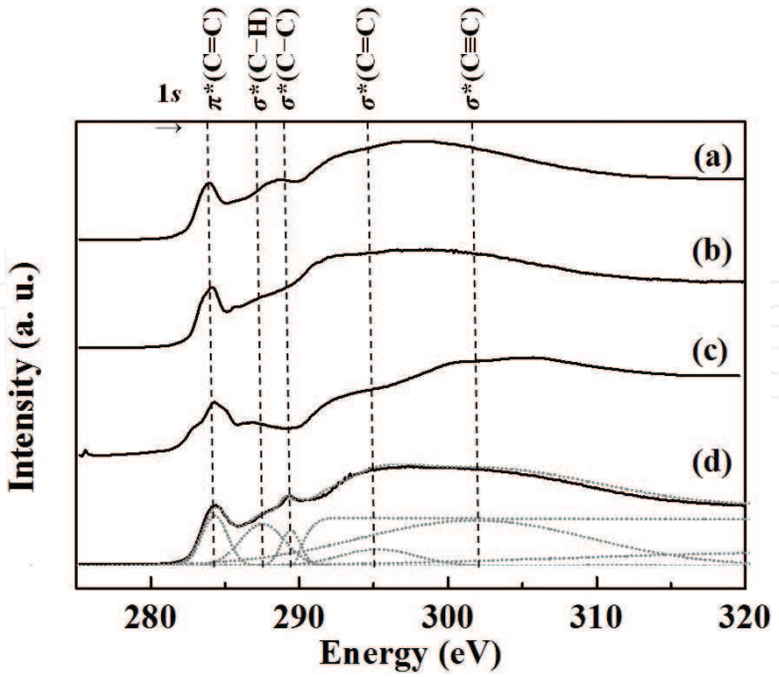

Figure 6. The carbon *K*-edge of NEXAFS spectra of DLC films deposited by (a) FCVA #6, (b) sputtering #8, (c) ECRCVD #9, and (d) PECVD #12.

in the DLC films. The sp^2 content of the DLC films can be extracted by normalizing the region of the resonance corresponding to the C 1 $s \rightarrow \pi^*$ at 284.6 eV with the whole spectral area. The absolute sp^2 content was evaluated by the purely sp^2 reference measured on the PG carbon *K*-edge as follows from which the $sp^3/(sp^3 + sp^2)$ ratio can be evaluated. The estimating error of the present fitting process is also around 5%. The $sp^3/(sp^3 + sp^2)$ ratios of DLC films were evaluated as listed in **Table 3** from the curve fitting of the NEXAFS spectra shown in **Figure 6(d)**.

The commercial software (HORIBA DelaPsi2) was used to simulate the SE data of standard materials and DLC films. **Figure 7** shows the typical fitting results of Ψ and Δ spectra of SE method with the application of the BEMA equations with different optical models. In the first stage, the optical models (c)–(h) using diamond as one of the basic standard materials were applied to the DLC films. The simulation results of sample #06 which has low-hydrogen content are shown in **Figure 7(a)** and **(b)**. The solid lines represent the experimental data, and the dashed lines the fitted data in each optical model. Except for Ψ of the model (c), the other simulation results were in good agreement with the experimental data. The χ^2 values of these simulations were 4.53, 0.93, 0.58, 0.89, 0.61, and 1.13, for the models of (c)–(h). The BEMA densities (ρ_{BEMA}) calculated by Eq. (1) using the models of (c)–(h) were 3.32, 2.39, 2.08, 2.32, 1.65, and 2.27 g/cm^3, respectively. The calculated ρ_{BEMA} of sample #06 using model (d) was close to the value of ρ_{XRR}. **Figure 7(c)** and **(d)** show the simulation of the Ψ, Δ spectra obtained from sample #11 using the same models (c)–(h), where the simulated spectra showed the large deviation from the experiments. The χ^2 of these fittings were 15.23, 4.15, 1.06, 0.84, 1.94, and 0.92 for the models of (c)–(h), respectively. The calculated ρ_{BEMA}

http://dx.doi.org/10.5772/intechopen.71727

Sample/group		Film type	H (at.%)	$sp^2/(sp^2+sp^3)$ (%)	n (λ = 550 nm)	k (λ = 550 nm)	$E_{n\text{-max}}$ (eV)	E_k (eV)	E_g (eV)	d (nm)	ρ (g/cm^3)
A	I	t*a*-C	0.3	47.9	2.65	0.13	3.45	0.70	0.68	207	3.25
B	I	t*a*-C	0.5	45.6	2.66	0.22	2.55	0.65	0.62	66	3.14
C	I	t*a*-C	1.0	44.3	2.75	0.30	2.00	0.75	0.71	181	3.23
D	II	*a*-C:H	19	56.6	2.34	0.31	1.60	0.65	0.61	312	2.17
E	II	*a*-C:H	19	59.1	2.42	0.29	1.90	0.80	0.76	186	2.21
F	III	*a*-C:H (PLC)	31	58.5	2.17	0.17	2.40	1.05	0.71	491	1.73
G	III	*a*-C:H (PLC)	32	67.1	2.15	0.19	2.20	1.00	0.89	501	1.72
H	III	*a*-C:H (PLC)	36	62.0	2.04	0.07	2.65	1.30	1.05	476	1.49
I	III	*a*-C:H (PLC)	37	64.9	1.97	0.05	2.30	1.15	0.92	457	1.43
J	III	*a*-C:H (PLC)	41	57.5	1.86	0.05	3.35	1.95	1.36	350	1.35
K	IV	PLC	45	63.0	1.65	0.00	4.80	2.60	2.55	254	1.21

Table 3. Hydrogen contents, $sp^2/(sp^2+sp^3)$ ratios, n, k, $E_{n\text{-max}}$, E_k, E_g, thickness (d), and true density (ρ) of DLC films, estimated from the analysis of RBS/ERDA, NEXAFS, SE spectra, and XRR profiles.

were 3.16, 2.42, 1.65, 1.73, 1.53, and 1.39 g/cm^3. Sample #11 obtained the optimal value of χ^2 in the case of model (f). Since samples #10–13 had high-hydrogen content, in the second stage, optical models (i)–(l) are PE adopted as the basic standard material and used to simulate the samples. The representative results of sample #13 are shown in **Figure 7(e)** and **(f)**. All the simulation data showed a good agreement with the experimental data (**Figure 7(e)** need to consider flipping up the raw data at part of 2.5–4.0 eV range to compare). The χ^2 of these fitting results using models (i)–(k) were 0.37, 0.36, and 0.33. The ρ_{BEMA} in these cases were 1.33, 1.20, and 1.23 g/cm^3. In addition, the volume fraction in the model (l) showed a negative value, being neglected in this chapter. ρ_{BEMA} of sample #13 has close agreement with ρ_{XRR} in the case of model (k). All the other ρ_{BEMA} and ρ_{XRR} of each sample are listed in **Table 2**.

In part two experiment, the RBS/ERDA, XRR, and NEXAFS analysis are also performed on all samples. All the results are summarized in **Table 3**. The film thicknesses are in the range of 66–501 nm. Samples A–C are hydrogen free (under 1.0 at.%) DLC films with high true density (exceed 3.10 g/cm^3). Samples D and E have the same hydrogen content of 19 at.% and almost the same true density of 2.20 g/cm^3. As the substrate bias decreases from 0.5 to 0 kV, the hydrogen contents of samples E and F increase from 31 to 45 at.% and their densities decrease from 1.73 to 1.21 g/cm^3. The estimated errors of these present fitting process are around 5%

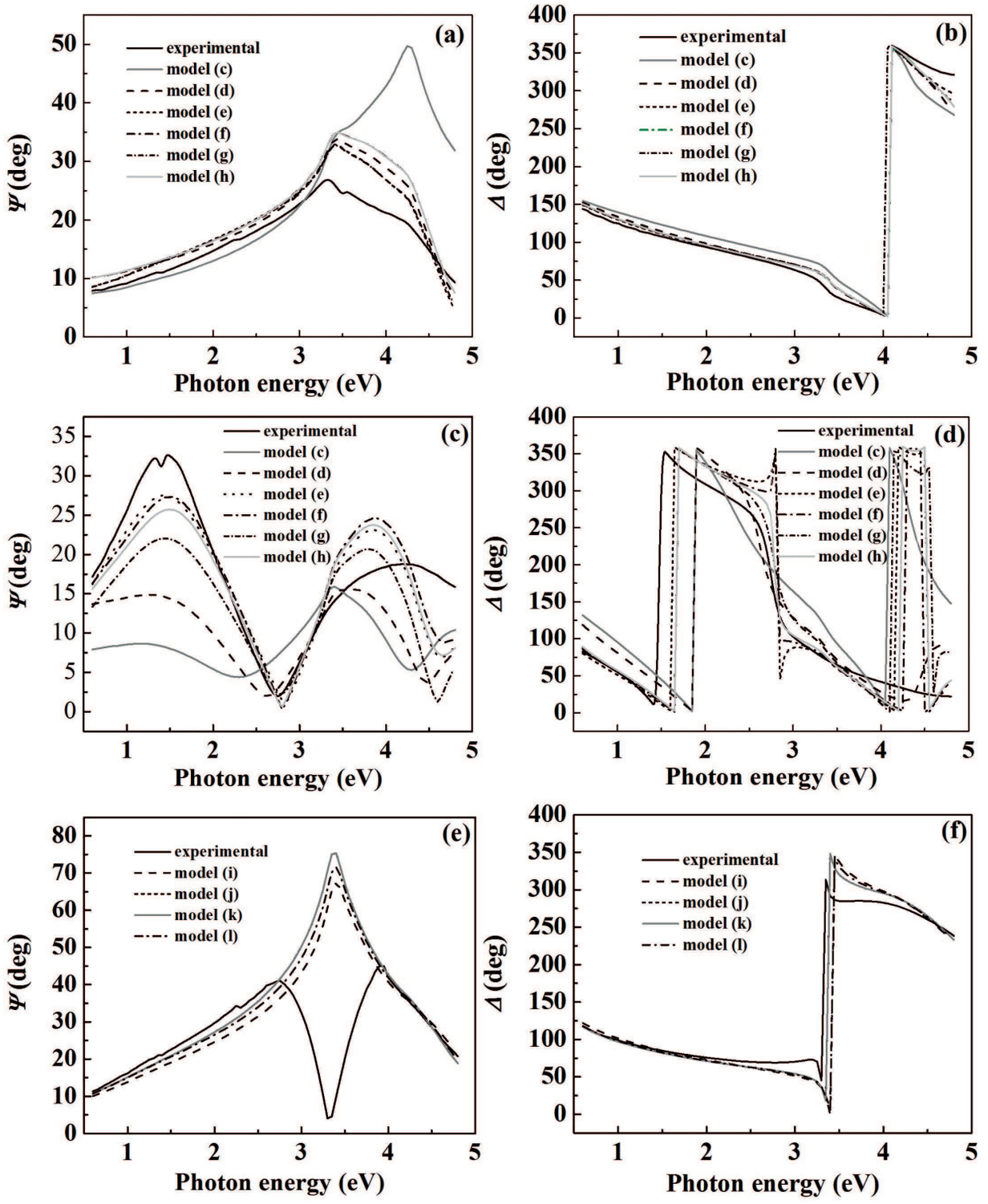

Figure 7. Representative simulation results of Ψ and Δ spectra of SE method applied BEMA equation with first six optical models (models (c)–(h) for FCVA #6 (a, b), PECVD #11 (c, d) methods). The other four optical models (models (i)–(l) for PECVD #13 (e, f) methods).

(e.g., sample F is 31 ± 2 at.%), ± 0.05 g/cm^3, and ±5 nm, respectively. According to our previous classification scheme, the present films can be well classified into three types: t*a*-C, *a*-C:H, and PLC films [14], although the boundary of hydrogen content between *a*-C: H and PLC films is still controversial.

Figure 8(a) shows the results of spectra of n in the photon energy range of 0.6–4.8 eV which is evaluated by using a three-layer optical model based on the Tauc-Lorenz and effective medium approximation model theory [11]. These films can be categorized into four groups based on the n at the energy of 2.25 eV (λ = 550 nm). Group includes samples A–C, where n is in the range of 2.65–2.75 and classified as t*a*-C films. Group includes samples D and E, where n is in the range of 2.34–2.42 and classified as *a*-C:H films. The difference between the minimum value of n in group and the maximum value of n in group is 0.17 and between its minimum value in group and maximum value in sample F is 0.16. In addition, the difference of n between samples J and K is 0.16, which is in the same degree with the above-mentioned differences. The difference between any other two samples is less than 0.1. Therefore, the sample K is categorized into groups, classified as PLC films in **Table 3**; the other samples are categorized into groups, classified as *a*-C:H or PLC films. Because the present grouping shows a good agreement with the classification of DLC films based on the hydrogen content, $sp^2/(sp^2 + sp^3)$ ratio, and true density, we validate that the gap between the four groups has a practical significance on the classification of DLC films.

Except for sample K with a maximum value of n at ≥4.8 eV [29], all the DLC films show the $E_{n\text{-max}}$ in the range of 0.6–4.8 eV as shown in **Figure 8(a)**. In this section, $E_{n\text{-max}}$ is defined

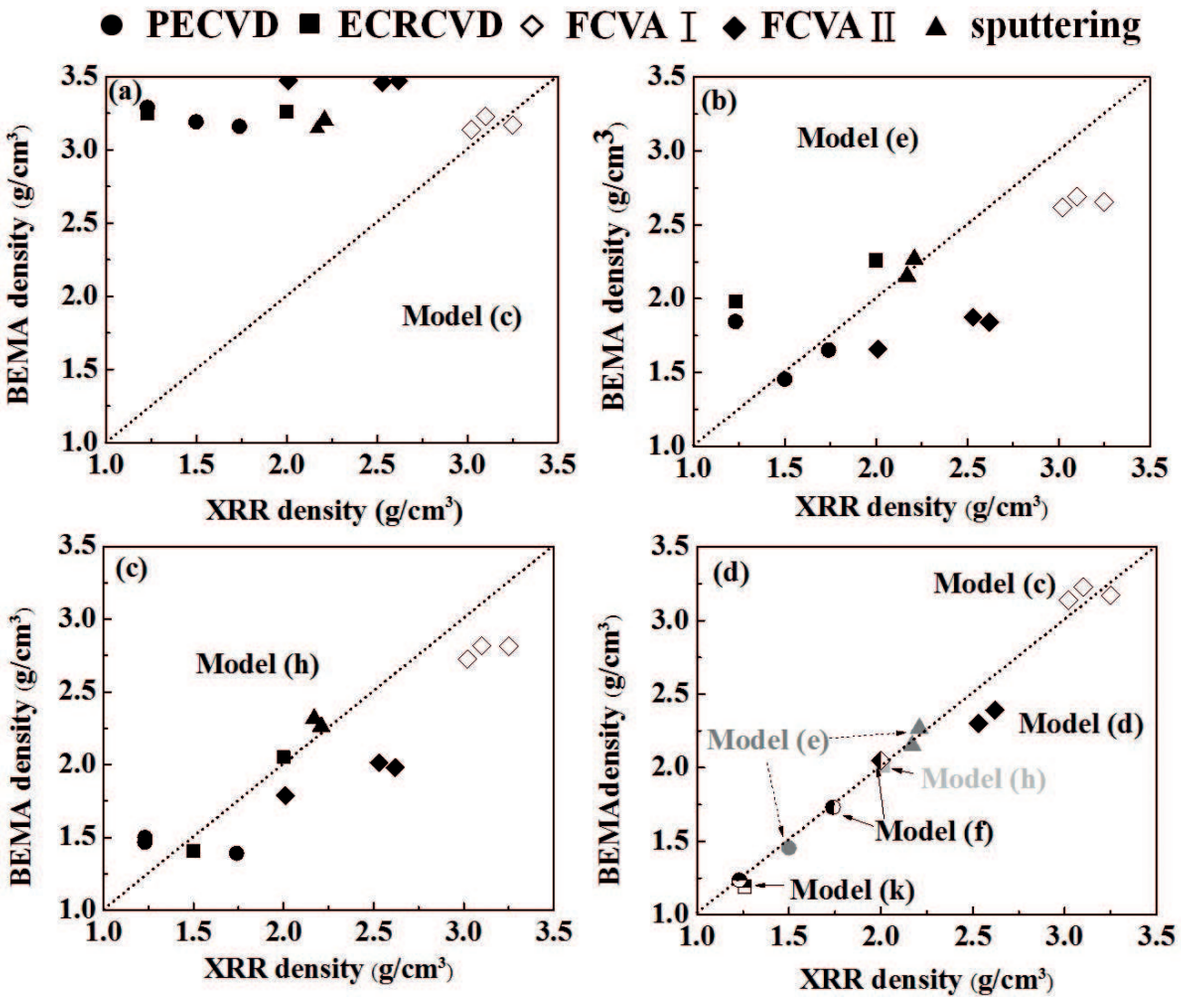

Figure 8. The spectra of n (a) and k (b) of DLC films in the photon energy range of 0.6–4.8 eV.

as the photon energy where n has the maximum value in the selected range. The $E_{n\text{-max}}$ for each sample is listed in **Table 3**. **Figure 8(b)** shows the k spectra of the samples A–K in the photon energy range of 0.6–4.8 eV. The k of each sample increases with photon energy. However, the k spectra have no distinct peak characteristic as seen in n. We focus on the threshold energy E_k defined as the photon energy where k has the value more than 10^{-4}. The optical energy gap E_g of DLC films is obtained from the Tauc-Lorentz model fitting of the experimental data.

4.2. Discussions

4.2.1. Discussions from experiment part one

Figure 9 shows the comparisons of ρ_{BEMA} with ρ_{XRR}. Optical models (c) and (d) without void will be useful for the high-density and low-hydrogen content DLC films as follows. **Figure 9(a)** indicates that all the simulation results with the model (c) have provided the ρ_{BEMA} values from 3.0 to 3.5 g/cm^3. Only the FCVA samples #01–03 are within this range and have small discrepancies with ρ_{XRR}. Model (c) is more suitable for the sample which has the density more than 3.0 g/cm^3 than model (d). Samples #04–06 have the hydrogen contents of about 5% which are considered to be the critical value between DLC films of types I and II or between types I and IV, leading to their densities (2.01–2.62 g/cm^3) lower than the samples #01–03. Our results suggest that the model (d) using GC instead of PG as the standard material of C(sp^2) is suitable for these samples. In models (e) and (f), the void is introduced as the free volume. **Figure 9(b)** shows the calculated results using model (e) for the samples #07, #08, and #12 which have the hydrogen contents in the range of 19–36 at.%. Since samples #05 and #11 result in the closed values with those of ρ_{BEMA} by using the model (f), it is also demonstrated that GC plays an important role in the simulation of the low-density DLC films. In models (g) and (h), PE was used as one of the standard materials. The calculated ρ_{BEMA} from the model (g) was lower than the observed ρ_{XRR} when ρ_{XRR} was less than 3.0 g/cm^3. Since

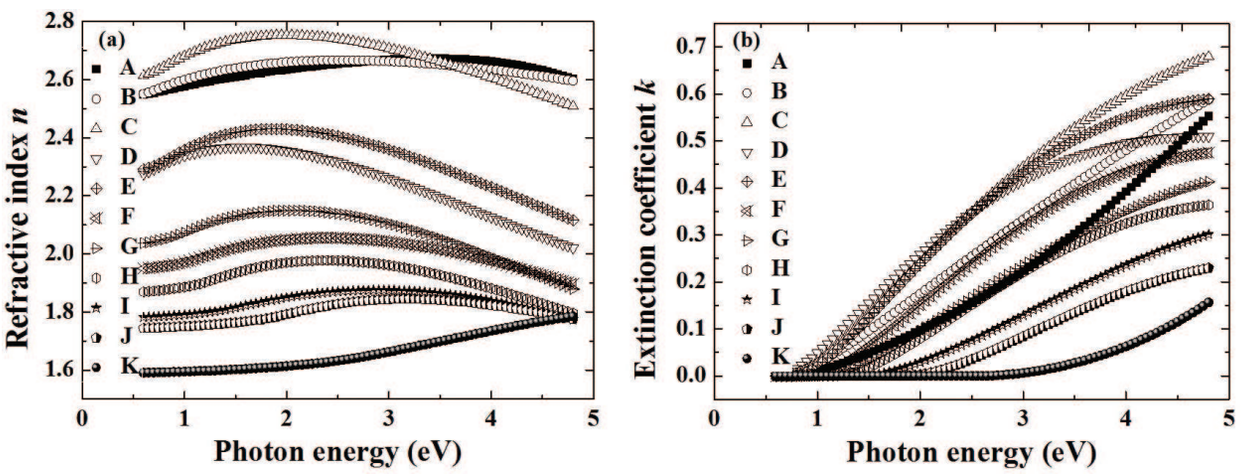

Figure 9. Comparison of ρ_{BEMA} and ρ_{XRR}, (a) model (c), (b) model (e), (c) model (h), (d) most suitable results in different optical models.

diamond has a similar dielectric function with PE, the low C(sp^3) (diamond) fraction and the low ρ_{BEMA} will be obtained when diamond and PE are simultaneously included. **Figure 9(c)** shows the results using model (h). Similar to model (g), almost all the samples showed lower ρ_{BEMA} than ρ_{XRR}. For samples #07–09, the ρ_{BEMA} values obtained from models (i)–(l) agree with ρ_{XRR}. We expect that high-hydrogen content samples, so-called PLC films, can be fully represented by these models. Samples #10 and #13 are appropriately represented by the model (k). Therefore, based on the above analysis and on the combination of the hydrogen content and ρ_{XRR} of all the samples, it can be concluded that each type of DLC film has the suitable optical model. First, it can be expected that the models (i)–(k) are the most suitable for low-density ($\rho_{XRR} < 1.4$ g/cm^3) and high-hydrogen content PLC films (type). The DLC films with the density in the range of $1.4 < \rho_{XRR} < 3.0$ g/cm^3 corresponding to the types can be simulated by the optical models (e) or (f). Besides, for the DLC films having similar ρ_{XRR} values, which are difficult to distinguish (e.g., samples #04 and #06), optical model (d) may be more suitable than the others. Furthermore, the type DLC films (hydrogen-free ta-C films) having the ρ_{XRR} values of more than 3.0 g/cm^3 are suitably simulated by the model (c). However, this chapter has not considered any other factors, such as the density of dangling bonds. Thus, there will be some errors or deviations between the simulation and measurement. **Figure 9(d)** shows the comparison of ρ_{BEMA} and ρ_{XRR}. All the BEMA simulations in the present chapter are fully consistent with the measured XRR results. It is therefore indicated that the volume fractions obtained by BEMA theory are the potential parameters for the structural analysis of DLC films.

Table 4 shows the $sp^3/(sp^3 + sp^2)$ ratios obtained by the fitting of carbon *K*-edge NEXAFS spectra and the volume fraction of each sample. The results show that each type of film has an ideal optical model corresponding to it, and there is no optical model to fit all types of DLC films. Simultaneously, the experimental data prove that the physical deposition method (FCVA or sputtering) is more likely to obtain ta-C and ta-C:H films and the chemical process (ECR or PECVD) more tends to deposit carbon films with higher hydrogen content. This is the fundamental reason why DLC films were able to show quite different physical and chemical properties. The $sp^3/(sp^3 + sp^2)$ ratios obtained from FCVA and sputtering methods have the close values, where the deviations of ratios are around ±0.1. The amount of hydrogen content may be the main reason for the division into the categories. When the hydrogen content exceeds about 25 at.%, PE may be more appropriate as the standard material of C(sp^3) than diamond because the deviations of $sp^3/(sp^3 + sp^2)$ ratios between BEMA and NEXAFS would be large (see the deviations from samples #07 and #08 to samples #11 and #12) if diamond used. In addition, in the simulation of sample #09, the optical model (h) was used where diamond, PG, and PE as the standard materials were simultaneously introduced. Although PE is artificially introduced as void, it has similar dielectric functions with a diamond which can also represent the C(sp^3) structure of the DLC films. The $sp^3/(sp^3 + sp^2)$ ratio of sample #09 is 0.49, where the volume fractions of diamond and PE obtained from this simulation analysis result almost in the same values of 33% and 32%. That is to say, even if the PE volume fraction is used, almost the same $sp^3/(sp^3 + sp^2)$ ratio may be obtained. Overall, the comparison between BEMA and NEXAFS

Sample	Type	Optical model	Volume fraction (%)			$sp^3/(sp^3 + sp^2)$ ratio	
			C(sp^3)	C(sp^2)	Void	BEMA	NEXAFS
#01	I	c	77	23	–	0.77	0.65
#02	I	c	70	30	–	0.70	0.58
#03	I	c	72	28	–	0.72	0.71
#04	II or III	d	39	61	–	0.39	0.49
#05	II or III	f	26	65	9	0.29	0.38
#06	II or III	d	32	68	–	0.32	0.47
#07	II or IV	e	34	42	24	0.44	0.50
#08	II or IV	e	39	39	22	0.50	0.57
#09	IV	h	33	35	32 (PE)	0.49	0.29
#10	VI	k	68 (PE)	24	8	0.74	0.42
#11	IV	f	21	58	21	0.27	0.38
#12	IV	e	7	54	40	0.11	0.42
#13	VI	k	49 (PE)	34	17	0.59	0.44

Table 4. Volume fraction and $sp^3/(sp^3 + sp^2)$ ratio of DLC films.

methods shows highly consistent results of the density and $sp^3/(sp^3 + sp^2)$ ratios for the films fabricated by the FCVA and sputtering methods which contain nonhydrogen precursors. When the hydrogen content increases the discrepancy of $sp^3/(sp^3 + sp^2)$ ratios between BEMA and NEXAFS tends to increase and two aspect reasons should be considered. First, in the present chapter, BEMA theory which is used to simulate the experimental data is taken into account only for the shading factors, where each optical model contains the physical combination of different standard materials; the density of dangling bond and the interface effects of different phases and other factors in DLC films have not been considered. Second, the experimental methods of the NEXAFS measurements should be taken into consideration. Usually, the total electron yield (TEY) and PEY modes are used in the measurement of NEXAFS. However, these modes are effective for the samples to have electrical conductivity; the DLC films, especially high-hydrogen content PLC films, have more complex structures close to the insulators, leading to the $sp^3/(sp^3 + sp^2)$ ratio less than the actual value [22]. Therefore, the present method of analysis can be used to distinguish the so-called DLC (type) and PLC films.

4.2.2. Discussion from experiment part two

Figure 10(a) shows the relationship between the present classification scheme based on n and k and the previous one based on the hydrogen contents and the $sp^2/(sp^2 + sp^3)$ ratios with some modifications. According to the later classification, our DLC films are categorized

http://dx.doi.org/10.5772/intechopen.71727

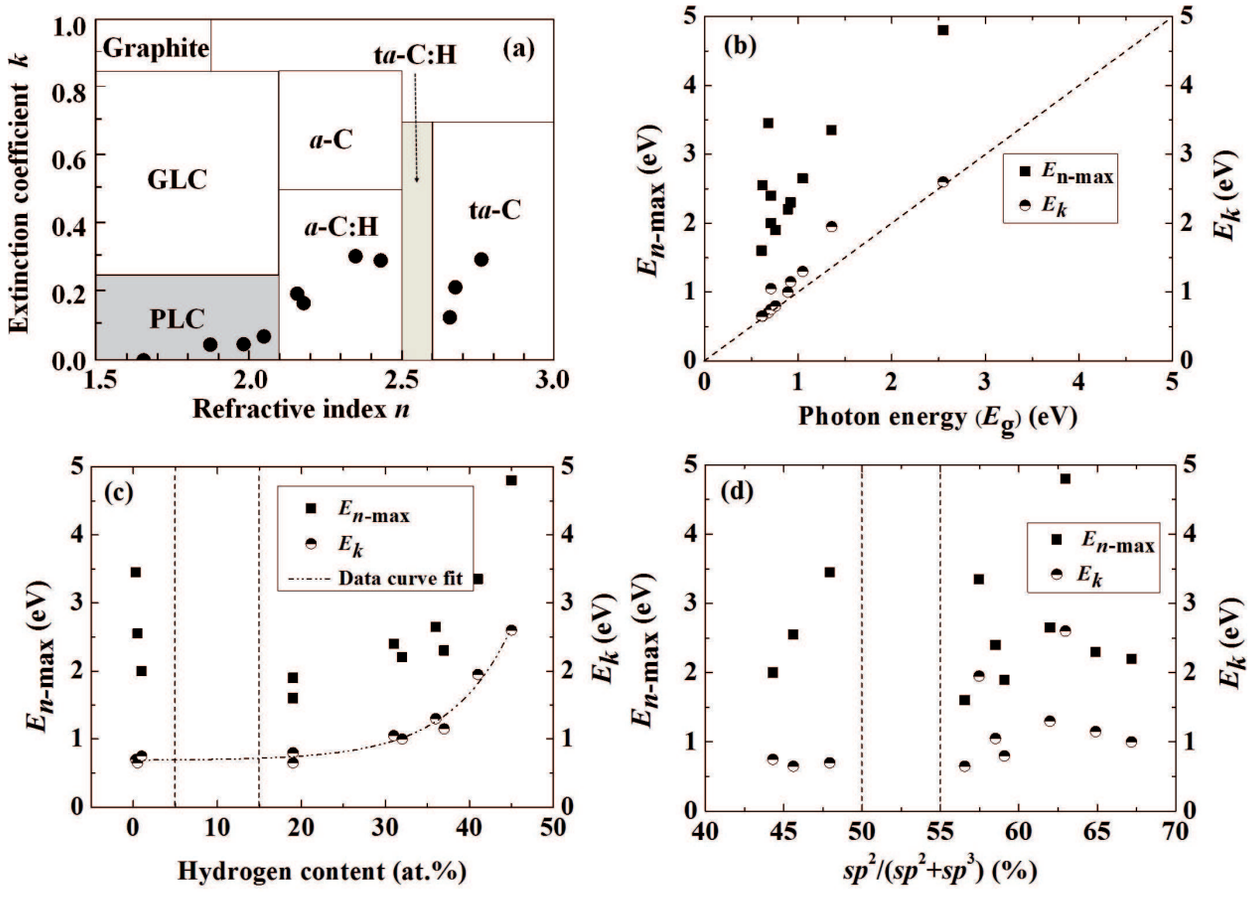

Figure 10. The relationship of (a) n and k over the classification of the deposited DLC films modified from past works [11, 12, 34] with wavelength at 550 nm; (b) Tauc-gap E_g and E_k or $E_{n\text{-max}}$; (c) hydrogen contents and E_k or $E_{n\text{-max}}$; (d) $sp^2/(sp^2 + sp^3)$ ratios and E_k or $E_{n\text{-max}}$.

into three types, however, the boundary between PLC and *a*-C:H is still controversial as specified in the range of n = 1.8–2.2 and k = 0.0–0.25 as shown in **Figure 10(a)**. It is necessary to construct a database which is large enough to establish the straightforward method to classify the DLC films in the future. E_g is often used to characterize practical optical properties of DLC materials [30]. **Figure 10(b)** shows E_k and $E_{n\text{-max}}$ as a function of E_g of the present samples. It is found that both E_k and $E_{n\text{-max}}$ are higher photon energy than its E_g. In particular, the E_k are distributed in the range of 0.65–2.60 eV and closed to E_g. In addition, we found that the hydrogen content and E_k have an exponential relationship and $E_{n\text{-max}}$ also exponentially increases in the hydrogen contents above 15 at.% as shown in **Figure 10(c)**. However, in **Figure 10(d)**, both E_k and $E_{n\text{-max}}$ seem to be an ambiguous correlation with the $sp^2/(sp^2 + sp^3)$ ratios. It might be explained in a way that, in the hydrogenated DLC films, C-H bond plays a crucial role in the cluster formation and its electrical conductivity rather than the $sp^2/(sp^2 + sp^3)$ ratio does [2, 5, 29], even though E_k and $E_{n\text{-max}}$ fairly link with E_g as shown in **Figure 10(b)**. It is noteworthy that a noticeable gap observed in the hydrogen content about 5–15% is possibly corresponding to the gap appeared in the $sp^2/(sp^2 + sp^3)$ ratios between about 50 and 55%. The hydrogen content tends to be a continuous distribution when it exceeds 20% [13, 31], while it seems to be a discontinuous distribution when it under 20% [32, 33]. The existence of the gaps should

be an important evidence and root cause that why the DLC films can be classified, and also corresponds to the results of the analysis in **Figure 10(a)**. Thus, the hydrogen content should be the decisive factor affecting the optical properties of DLC films. SE spectral analysis based on E_k and $E_{n\text{-max}}$ can facilitate the assessment of DLC films.

5. Conclusions

We analyzed various types of DLC films with different structure and hydrogen contents in the range of 0.3–42% fabricated by FCVA, sputtering, ECRCVD, and PECVD techniques. The structural analysis of a variety of DLC films was performed by using a combination of SE, BEMA, RBS/ERDA, NEXAFS, and XRR. In part one, from the comparisons of the density (ρ_{XRR} and ρ_{BEMA}) and $sp^3/(sp^3 + sp^2)$ ratio between BEMA simulation and NEXAFS results, we first established the appropriate optical models of the various types of DLC films and successfully made a detailed structural analysis of the selected DLC films. The results indicated that the BEMA method is effective for the structural analysis of samples. Especially in the so-called DLC films, good agreements are obtained between ρ_{BEMA} and ρ_{XRR} and between the $sp^3/(sp^3 + sp^2)$ ratios from BEMA and NEXAFS methods. Additionally, the hydrogen content plays a nonnegligible role in the structure of all types of DLC films; therefore, the method of the structural analysis of DLC films has to be carefully selected. In part two, through the analysis and comparison of structural analysis and optical constants, we have effectively classified different types of DLC films and achieved a high consistency. The results suggested that the optical constants (n and k, λ = 550 nm) obtained from SE could be a practical tool to classify the DLC films to some extent. The DLC classification method of optical constants based on SE analysis will be a most practical classification scheme which does not depend on large-scale analysis equipment. Simultaneously, we also found that E_k and $E_{n\text{-max}}$ of the present DLC films exhibit to have exponential dependencies on the hydrogen contents. In particular, the ellipsometrically measured E_k is useful to identify the hydrogen contents of the DLC films in the range from 0 to 50%. In summary, SE as a powerful analytical tool has great potential for simplifying the structural analysis of DLC films and achieving fast and efficient classification. The application of SE on the classification of DLC films need to pour enough attention; we also continue to focus on these research.

Author details

XiaoLong Zhou* and Hidetoshi Saitoh

*Address all correspondence to: zhou_xiaolong@mst.nagaokaut.ac.jp

Department of Materials Science and Technology, Nagaoka University of Technology, Japan

References

[1] Bewilogua K, Hofman D. History of diamond-like carbon films – From first experiments to worldwide applications. Surface and Coatings Technology. 2014;**242**:214-225

[2] Zhou XL, Tunmee S, Suzuki T, Phothongkam P, Kanda K, Komatsu K, Kawahara S, Ito H, Saitoh H. Quantitative NEXAFS and solid-state NMR studies of $sp^3/(sp^3 + sp^2)$ ratio in the hydrogenated DLC films. Diamond and Related Materials. 2016;**73**:232-240

[3] Ferrari AC, Libassi A, Tanner BK, Stolojan V, Yuan J, Brown LM, Rodil SE, Kleinsorge B, Robertson J. Density, sp^3 fraction, and cross-sectional structure of amorphous carbon films determined by x-ray reflectivity and electron energy-loss spectroscopy. Physical Review B. 2000;**62**(16):11089-11103

[4] Robertson J. Diamond-like amorphous carbon. Materials Science and Engineering R. 2002;**37**(4-6):129-281

[5] Jacob W, Möller W. On the structure of thin hydrocarbon films. Applied Physics Letters. 1993;**63**(13):1771-1773

[6] Gui WG, Lai QB, Zhang L, Wang FM. Quantitative measurements of sp^3 content in DLC films with Raman spectroscopy. Surface and Coatings Technology. 2010;**205**(7):1995-1999

[7] Tunmee S, Photongkam P, Euaruksakul C, Takamatsu H, Zhou XL, Wongpaya P, Komatsu K, Kanda K, Ito H, Saitoh H. Investigation of pitting corrosion of diamond-like carbon films using synchrotron-based spectromicroscopy. Journal of Applied Physics. 2016;**120**:195303

[8] Tunmee S, Supruangnet R, Nakajima H, Zhou XL, Arakawa S, Suzuki T, Kanda K, Ito H, Komatsu K, Saitoh H. Study of Synchrotron Radiation Near-Edge X-Ray Absorption Fine-Structure of Amorphous Hydrogenated Carbon Films at Various Thicknesses. Journal of Nanomaterials. 2015;**2015**:1-7

[9] VDI2840. Carbon films basic knowledge, film types and properties. Düsseldorf: Verein Deutscher Ingenieure; 2005

[10] Kim SW, Kim SG. Prospects of DLC coating as environment friendly surface treatment process. Journal of Environmental Sciences. 2011;**23**:S08-S13

[11] Hiramatsu M, Nakamori H, Kogo Y, Sakurai M, Ohtake N, Saitoh H. Correlation between Optical Properties and Hardness of Diamond-Like Carbon Films. Journal of Solid Mechanics and Materials Engineering. 2012;**7**(2):187-198

[12] DIN 50989-1: 2017-04-Draft, Ellipsometry-Part 1: Principles; Text in German and English, Beuth Verlag; 2017

[13] Weiler M, Sattel S, Jung K, Ehrhardt H, Veerasamy VS, Robertson J. Highly tetrahedral, diamond-like amorphous hydrogenated carbon prepared from a plasma beam source. Applied Physics Letters. 1994;**64**:2797-2799

[14] Zhou XL, Arakawa S, Tunmee S, Komatsu K, Kanda K, Ito H, Saitoh H. Structural analysis of amorphous carbon films by BEMA theory based on spectroscopic ellipsometry measurement. Diamond and Related Materials. 2017;**79**:46-59

[15] Niklasson GA, Granqvist CG, Hunderi O. Effective medium models for the optical properties of inhomogeneous materials. Applied Optics. 1981;**20**(1):26-30

[16] Chen ZY, Yu YH, Zhao JP, Wang X, Liu XH, Shi TS. Determination of the sp3/sp2 ratio in tetrahedral amorphous carbon films by effective medium approximation. Journal of Applied Physics. 1998;**83**(3):1281-1285

[17] Zhou XL, Suzuki T, Nakajima H, Komatsu K, Kanda K, Ito H, Saitoh H. Structural analysis of amorphous carbon films by spectroscopic ellipsometry, RBS/ERDA, and NEXAFS. Applied Physics Letters. 2017;**110**:201902

[18] Safaie P, Eshaghi A, Bakshi SR. Optical properties of oxygen doped diamond-like carbon thin films. Journal of Alloys and Compounds. 2016;**672**:426-432

[19] Papadopoulos AD, Anastassakis E. Optical properties of diamond. Physical Review B. 1991;**43**(6):5090-5097

[20] Tajir D, Tougaard S. Electronic and optical properties of selected polymers studied by reflection electron energy loss spectroscopy. Journal of Applied Physics. 2012;**111**(5):054101

[21] Guo WS, Wong SP, Yu YH. Spectroscopic ellipsometry characterization of diamond-like carbon films formed by filtered arc deposition. Nuclear Instruments and Methods in Physics Research Section B. 2000;**169**(1-4):54-58

[22] Battie Y, Broch L, En Naciri A, Lauret J-S, Guézo M, Loiseau A. Diameter dependence of the optoelectronic properties of single walled carbon nanotubes determined by ellipsometry. Carbon. 2015;**83**:32-39

[23] Fujiwara H. Spectroscopic Ellipsometry: Principles and Applications. London: John Wiley & Sons Ltd; 2007

[24] Palik ED. Handbook of Optical Constants of Solid. London: Elsevier; 1997

[25] Williams MW, Arakawa ET. Optical properties of glassy carbon from 0 to 82 eV. Journal of Applied Physics. 1972;**43**(8):3460-3463

[26] Iwaki M, Terashima K. Change in atomic density of glassy carbon by Na ion implantation. Surface and Coatings Technology. 2000;**128-129**:429-433

[27] Kawai T, Keller A. On the density of polyethylene single crystals. Philosophical Magazine. 2006;**8**(91):1203-1210

[28] Sauro JP, Bindell J, Wainfan N. Some Observations on the Interference Fringes Formed by X Rays Scattered from Thin Films. Physics Review. 1966;**143**:439-443

[29] Tamor MA, Haire JA, Wu CH, Hass KC. Correlation of the optical gaps and Raman spectra of hydrogenated amorphous carbon films. Applied Physics Letters. 1989;**54**:123-125

[30] Cho G, Yen BK, Klug CA. Structural characterization of sputtered hydrogenated amorphous carbon films by solid state nuclear magnetic resonance. Journal of Applied Physics. 2008;**104**:013531

[31] Tillmann W, Hoffmann F, Momeni S, Heller R. Hydrogen quantification of magnetron sputtered hydrogenated amorphous carbon (a-C:H) coatings produced at various bias voltages and their tribological behavior under different humidity levels. Surface and Coatings Technology. 2011;**206**:1705-1710

[32] Kaplan S, Jansen F, Machonkin M. Characterization of amorphous carbon-hydrogen films by solid-state nuclear magnetic resonance. Applied Physics Letters. 1985;**47**:750-753

[33] Ito H, Yamamoto K, Masuko M. Thermal stability of UBM sputtered DLC coatings with various hydrogen contents. Thin Solid Films. 2008;**517**:1115-1119

[34] Schneider D, Schwarz T. A photoacoustic method for characterising thin films. Surface and Coatings Technology. 1997;**91**:136-146

IntechOpen